Design and Development of a μ-Synthesis Controller for a Flexible Robotic Manipulator, Modelled as a Rotating Euler-Bernoulli Beam

Hamed Moradi, Gholamreza Vossoughi, Firooz Bakhtiari Nejad and Mohammad T. Ahmadian

Department of Mechanical Engineering, Sharif & Amirkabir Universities of Technology, Azadi Street, P.O. Box: 11155-9567, Tehran, Iran

(Received 26 September 2012; revised 14 February 2013; accepted 20 March 2013)

In this paper, a robust control strategy for a robotic manipulator, modelled as a cantilever rotating Euler-Bernoulli beam, is developed. Imprecision in the payload mass, unknown properties of the manipulator link, and torque disturbance are included as the sources of uncertainty. The objective is to achieve a desired angular rotation while the vibration of the manipulator tip is suppressed and the control system remains in a stable region. The control input of the system is an external driving torque. For formulation of the continuous system, the mode summation technique is used and equations of motion are described in the Laplace domain. Then, unstructured uncertainties are included in the form of multiplicative input uncertainty. The μ-synthesis control approach is used and an H_∞ optimal robust controller is developed based on the DK-iteration algorithm. Results show that the designed controller guarantees the robust stability and performance of the perturbed system against existing uncertainties. Consequently, stability of the closed-loop system, disturbance rejection, and trajectory tracking performance are achieved.

1. INTRODUCTION

Robotic manipulators are extensively used in areas such as industrial automation, underwater or space vehicles, manufacturing, material handling (e.g., CNC multi-axes milling machines), and medical surgeries. Flexible manipulators have several advantages over their rigid-arm counterparts, such as less material usage (and, consequently, less weight and energy consumption), smaller actuators, and more manoeuvrability. However, due to the inertia and external forces, light structures are more likely to deflect and vibrate. Therefore, the positioning inaccuracy of the end effector causes the performance of the manipulator to be unacceptable. Mechanical stiffening of the components has been used as a traditional solution to avoid such structural vibrations, which has proved to be ineffective for lightweight flexible manipulators. Consequently, the effects of link flexibility must be considered in the dynamic modelling, as stated by De Wit et al.[1] Thereafter, under external disturbances and parameter variations of the system, effective controllers are required to guarantee the quick and accurate manoeuvrability of manipulators.

Many research studies have been conducted to derive the equations of motion of flexible manipulators and to analyse their dynamics. In the early works, Book,[2] as well as Low and Vidyasagar,[3] derived the equations of motion for both rigid and flexible robot manipulators through Lagrangian formulation. To investigate the generic properties of the structural modelling related to the structural control, Spector and Flasher[4] used distributed sensors on the pinned-free Euler-Bernoulli beam. Choura et al.[5] found the differential equations describing the planar motion of a rotating, thin, flexible beam. Dynamics of a beam experiencing a combination of rotational and translational motions was analysed by Yuh and Young,[6] while its finite element simulation was presented by Gaultier and Cleghorn.[7] Dynamic equations for a planar manipulator with two flexible links, in contact with a constrained surface, have been studied by Matsuno et al.[8] Using Hamilton's principle, equations of motion for a chain of flexible links have been developed through a systematic procedure by Benati and Morro.[9] Damaren and Sharf[10] simulated the constrained motion of flexible-link manipulators, including inertial and geometric nonlinearities.

Fung and Chang[11] studied the dynamic modelling of a nonlinearly constrained flexible manipulator based on four configurations: Timoshenko, Euler, simple flexure, and rigid body beam theories. A linearised dynamic model for multi-link planar flexible manipulators with an arbitrary number of flexible links has been presented by Chen.[12] In that linearised model, flexible links were treated as Euler-Bernoulli beams and the Lagrangian approach was used to establish equations of motion. In addition, Meek and Liu[13] simulated the nonlinear dynamics of flexible manipulators under large overall motions. A study of modelling and the dynamic response of a multi-straight-line path tracing a flexible robot manipulator has been done by Kalyoncu[14] (under the action of an external driving torque and an axial force).

For performance control of the flexible robot manipulators, many control techniques have been developed based on the Euler-Bernoulli beam theory. Point-to-point position control of a flexible beam using the Laplace transform technique has been done by Bhat and Miu.[15] Diken[16] investigated the vibration control of the beam using measured shear force as the feedback, and simultaneously achieved the desired angular rotation by using a PD controller. Implementation of a neural network tracking controller for a single flexible link has been compared for PD and PID controllers by Gutierrez et al.[17] Due

to a simple control structure, easy implementation, less real-time computational load, and low cost, traditional PID controllers have been extensively used in industrial operations, such as the works done by Gutierrez et al.[17] and A-Ramirez et al.[18]

When a classical controller in the family of PI/PD or PID is designed for a specific dynamic system, and its control gains are tuned appropriately, the desired performance is achieved with bounded values of control efforts. However, in the presence of structured/unstructured model uncertainties, very large actuations are required to achieve precise control and improve the transient performance (in many cases, actuator saturation occurs). This phenomenon has been generally observed in other dynamic systems or processes, as seen in Skogestad and Postlethwaite.[19] Therefore, developing a robust tuning procedure that guarantees the transient performance of robot manipulators is a study that requires further investigation.

Many tracking control algorithms have been developed to make each joint track a desired trajectory. In an early work for the Timoshenko beam, and to achieve tracking with suppression of elastic vibrations, Yuan and Hu[20] designed a non-linear controller using input-output linearization and elastic mode stabilization. Green and Sasiadek[21] studied the dynamics and tracked the optimal control of a two-link flexible manipulator, while Onsay and Akay[22] investigated the vibration reduction of a flexible arm by time optimal control. However, in optimal control approaches, accurate selection of switching time is required (which depends on the system dynamics). Therefore, minor modelling errors cause switching errors and consequently lead to a significant increase in the residual vibrations.

In the field of adaptive control, variable structure set-point control of under-actuated robots—as seen in Su and Leung[23] and Su and Stepanenko[24]—and nonlinear adaptive control via the sliding mode state and perturbation observer, per Jiang and Wu,[25] have been done. However, in these control approaches, a fixed control law is designed based on the priori bound of uncertainty. In addition, for the tracking objective, Huang et al.[26] developed a guaranteed performance adaptive algorithm with limited torque, and Slotine and Li[27] investigated the composite adaptive control for robot manipulators. However, adaptive control techniques are potentially complex and utilize design methods that require *a priori* knowledge of the system model, as seen in Kirchoff and Melek.[28] Therefore, although adaptive control approaches lead to fine control and compensate for structured uncertainties of the manipulators dynamics, they usually fail to appropriately work in the presence of unstructured uncertainties.

Recently, many works have been presented to deal with the problem of the fuzzy control of robot manipulators; e.g., Ha et al.[29] developed a fuzzy sliding mode control. Castillo and Melin[30] used a hybrid fuzzy-neural approach for an intelligent adaptive model-based control of robotic systems. Neuro-fuzzy control of modular and reconfigurable manipulators, as seen in the work of Melek and Goldenberg,[31] and robust control of a spatial robot using fuzzy sliding modes, as appears in Yagiz and Hacioglu,[32] have been investigated. In these neuro-fuzzy control approaches, control law is changed according to certain predefined rules, which depend on the position of the system error states with respect to sliding surfaces. However, implementation of controllers developed based on these methods requires achieving data for structure identification, and designing its control parameters demands a substantial amount of time.[28]

Robot manipulators as multivariable coupling systems are usually associated with structured and unstructured uncertainties. Imprecision in the payload mass, unknown properties of the manipulator link, and torque disturbance are the sources of structured uncertainties. High frequency parts of the dynamics and un-modelled dynamics, such as disturbance and nonlinear friction, cause the unstructured uncertainties. In contrast with the adaptive and fuzzy based controllers, robust controllers require no accurate knowledge of the system, and their implementation is convenient (an early survey of robust control for robot manipulators has been presented by Sage et al.[33]). Besides the robust-fuzzy[32] and robust-adaptive based control approaches using Lyapunov's direct method,[26,34] nonlinear H_∞ or mixed H_2/H_∞ control techniques have been developed by Siqueria et al.[35] and Chen et al.[36] Moreover, Karkoub and Tamma[37] studied the μ-synthesis control of flexible manipulators, modelled after the Timoshenko beam theory.

As it is discussed, various strategies have been implemented to solve the tracking problem of manipulators. However, a simultaneous analysis to achieve the desired tracking and vibration suppression while keeping the closed-loop controlled system globally stable has not been investigated, especially when the dynamic model associates with various uncertainties. Therefore, there is still room for a comprehensive control analysis of the problem in the presence of model uncertainties.

In this paper, a robotic manipulator is modelled as a cantilever rotating Euler-Bernoulli beam. To analyze the problem, the mode summation technique is used and equations of motion are described in the Laplace domain. The model is associated with parametric uncertainties caused by imprecision in the payload mass and unknown properties of the manipulator link. After representation of the uncertain system in the form of general control configuration, uncertainties are included in the form of multiplicative input uncertainty. The μ-synthesis control approach is used and an H_∞ robust controller is developed based on the DK-iteration algorithm. Unlike the previous works, both desired angular rotation and suppression of manipulator tip vibration are achieved by manipulation of an external driving torque, as the control input. Simulation results of the manipulator response are presented in the time and frequency domains. Results show that the designed controller guarantees the robust stability and performance of the perturbed system against existing uncertainties.

2. DYNAMICS OF THE ROBOTIC MANIPULATOR

The physical configuration of the single-link flexible manipulator is shown in Fig. 1 where UOV and xoy represent stationary and moving coordinate frames, respectively. The arm and the joint of the manipulator are assumed to be flexible. To simulate the effect of a gripped payload, a mass attached to the arm tip is considered. With the assumption of a long and slender manipulator, transverse shear and rotary inertia effects are neglected. Therefore, the Euler-Bernoulli beam theory can be used to model the elastic behaviour of the manipulator, per Mohamed and Tokhi.[38] In addition, the mass and flexible properties are assumed to be distributed uniformly along the flexible link. According to the formulation developed by White and Heppler,[39] by neglecting the effect of shear, the equations

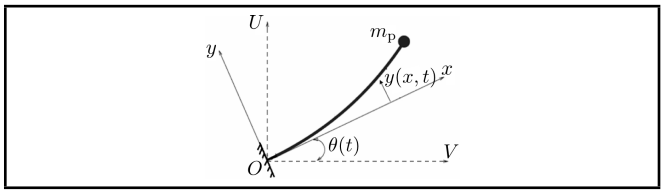

Figure 1. Schematic of the flexible manipulator.

of motion for the Timoshenko beam are reduced for the Euler-Bernoulli one as follows:[16]

$$EI\frac{\partial^4 y(x,t)}{\partial x^4}+\rho\frac{\partial^2 y(x,t)}{\partial t^2}=\rho x\frac{\partial^2\theta}{\partial t^2}-m_{\rm p}\frac{\partial^2 y(l,t)}{\partial t^2}; \quad (1)$$

$$J_{\rm tot}\frac{\partial^2\theta}{\partial t^2}+\int_0^t\rho\left(\frac{\partial^2 y(x,t)}{\partial t^2}\right)xdx+m_{\rm p}l\frac{\partial^2 y(l,t)}{\partial t^2}=\tau; \quad (2)$$

$$J_{\rm tot}=\frac{J_{\rm m}}{n^2}+J_{\rm b}.$$

For Eqs. (1) and (2), EI is the flexural rigidity, y is the beam deflection measured with respect to the xoy coordinate, ρ is the mass per unit length, $m_{\rm p}$ is the payload mass, θ is the rotational angle, and τ is the motor torque with respect to the beam axis. In the aforementioned equations, $J_{\rm tot}$ is the total mass moment of inertia including the motor inertia $J_{\rm m}$ and the beam inertia $J_{\rm b}$, and n is the gear ratio between the beam and motor rotational angles. Beam deflection at any point x can be expressed in terms of the normal modes $\phi_i(x)$ as follows:[40]

$$y(x,t)=\sum_i q_i(t)\phi_i(x); \quad (3)$$

where $q_i(t)$ is the i-th generalized coordinate. For a cantilever Euler-Bernoulli beam, the eigenvector at any mode is given as[40]

$$\phi_i(x)=A_i[\cosh\lambda_i x-\cos\lambda_i x-\mu_i(\sinh\lambda_i x-\sin\lambda_i x)]; \quad (4)$$

$$\mu_i=(\cosh\lambda_i+\cos\lambda_i)/(\sinh\lambda_i+\sin\lambda_i) \quad (5)$$

and the natural frequencies of a cantilever beam are defined as

$$\omega_i=\left(\frac{\lambda_i}{l}\right)^2\sqrt{\frac{EI}{\rho}}; \quad (6)$$

where values of λ_i are constants taking values of $\lambda_1=1.88$, $\lambda_2=4.69$, and $\lambda_3=7.85$ for the first three natural frequencies. Normal modes, $\phi_i(x)$, are orthogonal functions that satisfy the following relationship:

$$A_i^2\int\phi_i(x)\phi_i(x)=1. \quad (7)$$

Substituting Eqs. (4) and (5) in Eq. (7) results in $A_i=1$. Substituting Eq. (3) in Eq. (1) and multiplying the resulting equation by $\phi_j(x)$, as well as using the orthogonal characteristics of the modes as

$$\int_0^l\phi_i(x)\phi_j(x)dx=\begin{cases}1 & \text{for } i=j\\ 0 & \text{for } i\neq j\end{cases} \quad (8)$$

yields

$$\ddot{q}_i+\tilde{\omega}_i^2 q_i=\alpha_i^*\ddot{\theta} \quad (9)$$

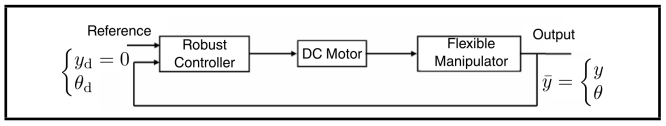

Figure 2. General schematic of the closed-loop control system.

and

$$\tilde{\omega}_i^2=\frac{\omega_i^2}{1+\Gamma_i}; \quad (10)$$

$$\alpha_i^*=\frac{1}{1+\Gamma_i}\frac{\int_0^l x\varphi_i(x)dx}{\int_0^l\varphi_i^2(x)dx}; \quad (11)$$

$$\Gamma_i=\frac{m_{\rm p}}{\rho}\frac{\int_0^l\varphi_i(l)\varphi_i(x)dx}{\int_0^l\varphi_i^2(x)dx}. \quad (12)$$

Similarly, substituting Eq. (3) in Eq. (2) yields

$$\ddot{\theta}+\sum\gamma_i\ddot{q}_i=\frac{\tau}{J_{\rm tot}} \quad (13)$$

and

$$\gamma_i=\frac{1}{J_{\rm tot}}\left\{\rho\int_0^l x\varphi_i(x)dx+m_{\rm p}l\varphi_i(l)\right\}. \quad (14)$$

Multiplying Eq. (13) by α_i^*, and substituting $\alpha_i^*\ddot{\theta}$ from Eq. (9) yields

$$\beta_i(\ddot{q}_i+\tilde{\omega}_i^2 q_i)+\sum_j\eta_j\ddot{q}_j=\tau \quad (15)$$

and

$$\beta_i=\frac{J_{\rm tot}}{\alpha_i^*}; \quad (16)$$

$$\eta_j=J_{\rm tot}\gamma_j; \quad (17)$$

while transforming Eq. (15) into the Laplace domain results in

$$\beta_i(s^2+\tilde{\omega}_i^2)Q_i(s)+\sum_j\eta_j s^2Q_j(s)=\tau(s). \quad (18)$$

Expanding Eq. (18) for two modes ($i,j=1,2$) (the reason for considering two modes is discussed next in section 4) and solving the set of equations for $Q_1(s)$ and $Q_2(s)$ yields the following:

$$\begin{bmatrix}Q_1(s)\\ Q_2(s)\end{bmatrix}=\frac{\tau(s)}{D(s)}\cdot \cdot\begin{bmatrix}(\beta_2+\eta_2)s^2+\beta_2\tilde{\omega}_2^2 & -\eta_2 s^2\\ -\eta_1 s^2 & (\beta_1+\eta_1)s^2+\beta_1\tilde{\omega}_1^2\end{bmatrix}\begin{bmatrix}1\\ 1\end{bmatrix}; \quad (19)$$

$$D(s)=[(\beta_1+\eta_1)s^2+\beta_1\tilde{\omega}_1^2][(\beta_2+\eta_2)s^2+\beta_2\tilde{\omega}_2^2]-\eta_1\eta_2 s^4. \quad (20)$$

3. H_∞ ROBUST CONTROL DESIGN

Figure 2 shows a general schematic of the designed closed-loop control system and its components are described in a schematic of the H_∞ control design, shown in Fig. 3. Variables r, $\bar{y}$, e, u, d, and d_i are the reference input, output variables, tracking error, controlled system input, output disturbance, and input disturbance, respectively. Signals $\tilde{y}$, $\tilde{e}$, and $\tilde{u}$ are weighted with the weighting functions $W_{\rm m}$, $W_{\rm p}$, and $W_{\rm u}$.

According to the Fig. 3, the transfer function between the output and the disturbance (y/d), and between the tracking

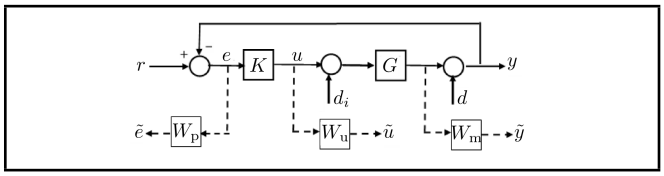

Figure 3. Components of the H_∞ control design.

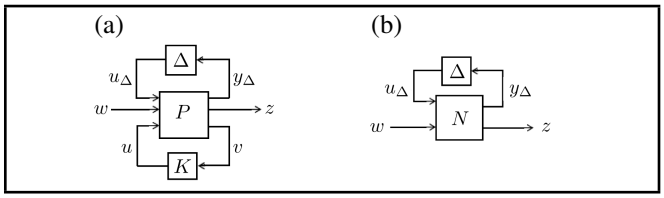

Figure 4. General control configuration in the presence of model uncertainty is used for (a) synthesis (b) analysis.

error and the reference input (e/r), is explained by $S = (I + GK)^{-1}$, which is called the sensitivity transfer function. Moreover, the complementary sensitivity function, $T = GK(I + GK)^{-1}$, describes the transfer function between the output and the reference input (y/r). In addition, the control signal is explained in terms of the reference input, output, and input disturbance as $u = KS(r - d - Gd_i)$. Consequently, to achieve disturbance rejection and appropriate transient performance, $\|S\|_\infty$ must be small while for the perfect tracking, $|T(j\omega)|$ must have unit value (because for perfect tracking, $y = r$.

At low frequencies, the performance weight W_p must be large enough to achieve a desired nominal performance. At high frequencies, the upper bound function W_m on the possible multiplicative uncertainties must be large enough. Due to the constraint $S + T = I$ (identity), it is not possible to make both of them simultaneously small. Therefore, the weighted sensitivity function, $\|W_p S\|_\infty$, and complementary sensitivity function, $\|W_m T\|_\infty$, are minimized. In addition, to restrict the magnitude of the control effort, the upper bound $1/|W_u|$ on the magnitude of KS must be small. To achieve these conditions, a stacking mixed sensitivity approach is used, as follows:

$$\|N\|_\infty = \max_\omega \bar{\sigma}(N(j\omega)) < 1;$$

$$N = \|W_p S \quad W_u KS \quad W_m T\|_\infty.$$

At each frequency, the size of the matrix N is determined by computing the maximum singular value $\bar{\sigma}(N(j\omega))$. The stabilizing H_∞ optimal controller is determined by minimizing the function $\|N(K)\|_\infty$.[19]

3.1. General Control Configurations in Terms of $N - \Delta$ Structure

To include the existing uncertainties in the closed-loop system shown in Fig. 2, the general control configuration is used, as shown in Fig. 4, where P and K are the generalized plant and controller. Possible perturbations are included in the block diagonal matrix Δ, which is normalized such that $\|\Delta\|_\infty \leq 1$. The block diagram of Fig. 4a, in which P is closed through a lower loop by K, is transformed into the block diagram in terms of N as shown in Fig. 4b. Using lower linear fractional transformation (LFT) results in (see Appendix A):

$$N = F_L(P, K) = P_{11} + P_{12}K(I - P_{22}K)^{-1}P_{21}.$$

Using an upper linear fractional transformation (LFT) for the N_Δ structure, the perturbed (uncertain) transfer function from external inputs w to external outputs z is evaluated as

$$z = F_u(N, \Delta)w; \tag{21}$$

$$F_u(N, \Delta) = N_{22} + N_{21}\Delta(I - N_{11}\Delta)^{-1}N_{12}. \tag{22}$$

3.2. Stability and Performance Analysis for the Uncertain System

The structured singular value μ is used to analyze nominal performance (NP), robust stability (RS), and robust performance (RP) of the uncertain system (see Appendix B). After representation of the uncertain system in the form of $N - \Delta$ structure, using Eqs. (21) and (22), and considering the RP requirement as $\|F\|_\infty \leq 1$ for all possible perturbations, the conditions of nominal stability/performance and robust stability/performance become[19]

$$NS \Leftrightarrow N \text{ (internally stable)}; \tag{23}$$

$$NP \Leftrightarrow \bar{\sigma}(N_{22}) = \mu_{\Delta_P} < 1, \ \forall\omega, \text{ and } NS; \tag{24}$$

$$RS \Leftrightarrow \mu_\Delta(N_{11}) < 1, \ \forall\omega, \text{ and } NS; \tag{25}$$

$$RP \Leftrightarrow \mu_{\hat{\Delta}}(N) < 1, \ \forall\omega, \text{ and } NS; \tag{26}$$

$$\hat{\Delta} = \begin{bmatrix} \Delta & 0 \\ 0 & \Delta_P \end{bmatrix}; \tag{27}$$

$$N = \begin{bmatrix} W_m T_I & W_I KS \\ W_p SG & W_p S \end{bmatrix}; \tag{28}$$

and

$$T_I = KG(I + KG)^{-1}; \tag{29}$$

$$S = (I + GK)^{-1}; \tag{30}$$

where the detailed structure of the block diagonal matrix Δ depends on the existing uncertainty and Δ_P is always a full complex matrix, indicating the H_∞ performance specification.

4. SIMULATION OF THE CONTROL DESIGN, RESULTS, AND DISCUSSION

The mass and flexible properties are assumed to be distributed uniformly along the flexible manipulator. For physical simulation of the problem, a steel type flexible manipulator of dimensions $1000 \times 30 \times 2.5\,\text{mm}^3$, Young's modulus of the elasticity $E = 210 \times 10^9\,\text{N/m}^2$, area moment of inertia $I = 39.1\,\text{mm}^4$, mass density per length $\rho = 0.585\,\text{kg/m}$, and mass moment of inertia of beam $J_b = 0.195\,\text{kg m}^2$ with payload mass of $m_p = 0.25\,\text{kg}$ is considered. With the assumption of the ratio $J_m/J_b n^2$ to be the unit, the total mass moment of inertia becomes $J_{tot} = 2J_b = 0.39\,\text{kg m}^2$. Consequently, according to the governing equations in the modelling section, the nominal values of the parameters for the two first modes of the flexible arm, given by Eqs. (10)–(12) and (16)–(17), are found as follows:

$$\bar{\beta}_1 = 1.15, \tag{31}$$

$$\bar{\beta}_2 = 2.68, \tag{32}$$

$$\bar{\eta}_1 = 0.83, \tag{33}$$

$$\bar{\eta}_2 = -0.45, \tag{34}$$

$$\bar{\tilde{\omega}}_1 = 10.2, \tag{35}$$

$$\bar{\tilde{\omega}}_2 = 104.1. \tag{36}$$

It should be mentioned that according to Eq. (6), the natural frequencies of the considered cantilever beam are proportional with the coefficients $\lambda_i^2, i = 1, 2, 3, \ldots$, while $\lambda_1 = 1.88$, $\lambda_2 = 4.69$, and $\lambda_3 = 7.85$. Consequently, the second and third natural frequencies (ω_2, ω_3) are about 6 and 17 times of the first one (ω_1). These frequencies are sufficiently far away from the first natural frequency. Under such conditions and for the considered model here, the higher modes are not excited (and if excited, have a negligible effect on time responses of the dynamic system). Therefore, considering two modes in the expansion of Eq. (18) is physically enough (even in prior research[16]only one mode was considered).

However, it should be noted that for other cases of robotic manipulators, in which the flexural rigidity is reduced greatly, the inclusion of higher modes is necessary. In that case, the procedure used in this research can be easily extended in a straight forward manner to the models with higher numbers of modes.

4.1. Description of the Uncertain Model

The various sources of model uncertainty are classified into parametric (real) and dynamic (frequency-dependent). The first type occurs when the model structure is known, but some of the parameters are uncertain. The second type is caused by the missing dynamics, usually at high frequencies where the model is in error. In this paper, the imprecision in the payload mass and unknown properties of the manipulator link are considered as the parametric uncertainties. As a real case study, assume that the physical parameters of the manipulator and payload mass are varied around their nominal values so that it results in variation of parameters, e.g., with $\pm 25\%$ uncertainty as follows:

$$0.75\bar{\chi} < \chi < 1.25\bar{\chi} \tag{37}$$

where χ can take any values of β_i, η_i, and $\tilde{\omega}_i$, $i = 1, 2$ for the two first modes of the flexible manipulator, given by Eqs. (31)–(36).

4.2. Complex Uncertainty and Performance Weight Functions

Frequency domain analysis is used to quantify the parametric uncertainties, resulting in complex perturbations normalized as $\|\Delta\|_\infty \leq 1$. In many practical cases, the configuration of multiplicative input uncertainty is used to represent the various sources of dynamic uncertainty, as shown in Fig. 5. In this approach, the perturbed plant $G_{\rm p}(s)$ is described as

$$G_{\rm p}(s) = G(s)[1 + W_{\rm m}(s)\Delta_{\rm I}(s)]; \quad \underbrace{|\Delta_{\rm I}(j\omega)| \leq 1 \ \forall\omega}_{\|\Delta_{\rm I}\|_\infty \leq 1}$$

where the $G(s)$ is the nominal plant and $\Delta_{\rm I}(s)$ is any stable transfer function with a magnitude less or equal to 1, at each frequency. The original complex uncertainty $G_{\rm p}(s)$ is replaced by a conservative disc type approximation $G'_{\rm p}(s)$ of

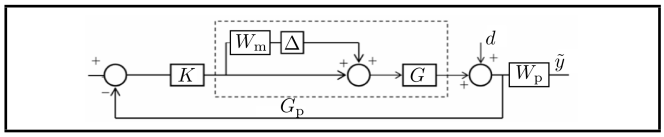

Figure 5. Uncertain plant including multiplicative input uncertainty.

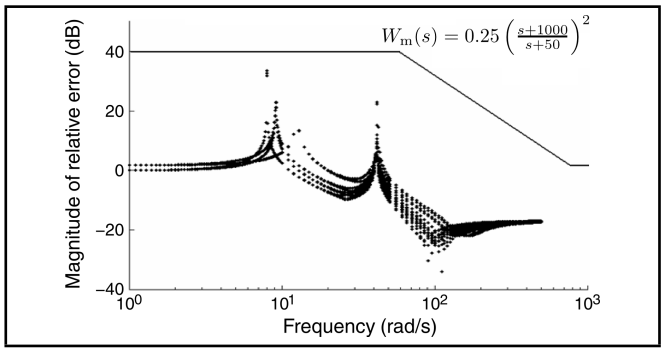

Figure 6. Relative errors $|(G_{\rm p} - G)/G|$ for 2^6 perturbed plants.

radius $|W_{\rm m}(j\omega)G(j\omega)|$, where the weight function $W_{\rm m}$ is determined as[19]

$$l_{\rm I}(\omega) = \max_{G_{\rm p}\in\Pi} \left|\frac{G_{\rm p}(j\omega)}{G(j\omega)} - 1\right|, \quad |W_{\rm m}(j\omega)| \geq l_{\rm I}(\omega), \ \forall\omega,$$

where Π is the set of possible perturbed plants and $G(s)$ is a 2×2 matrix given by Eqs. (19) and (20). As shown in Fig. 6, the relative plant errors $|G_{\rm p}/G - 1|$ are plotted for 2^6 possible perturbed plants (because any of parameters β_i, η_i, and $\tilde{\omega}_i$, $i = 1, 2$ can take two extreme limits, given by Eqs. (31)–(36) and (37)), where some plots are coincide. According to this figure, the weight function of the model uncertainty, the upper bound on relative error functions, is found as

$$W_{\rm m}(s) = 0.25\left(\frac{s + 1000}{s + 50}\right)^2. \tag{38}$$

At the low frequencies, the weight function $1/|W_{\rm P}|$ as the upper bound on the sensitivity function $|S|$ is equal to the parameter A (typically $A \approx 0$) in correlation with the steady state tracking error. At the high frequencies, it approaches to the maximum peak amplitude $M \geq 1$, and the bandwidth frequency ($\omega^*_{\rm B}$) indicates the speed of the time response. An appropriate performance weight $W_{\rm P}$ is described in terms of these parameters as[19]

$$W_{\rm P} = \frac{s/M + \omega^*_{\rm B}}{s + \omega^*_{\rm B} A}.$$

For instance, to have a desired step response with a maximum overshoot of 10 percent, the rise time of about 1.5 s, and a perfect tracking (error ≈ 0), the performance weight is selected as

$$W_{\rm P}(s) = \frac{s/1.1 + 1.82}{s + 2 \times 10^{-4}}. \tag{39}$$

4.3. μ-Synthesis Controller Design Based on the DK-iteration Algorithm

In the robust H_∞ technique, DK-iteration is an effective practical approach used to find the μ-optimal controller. In

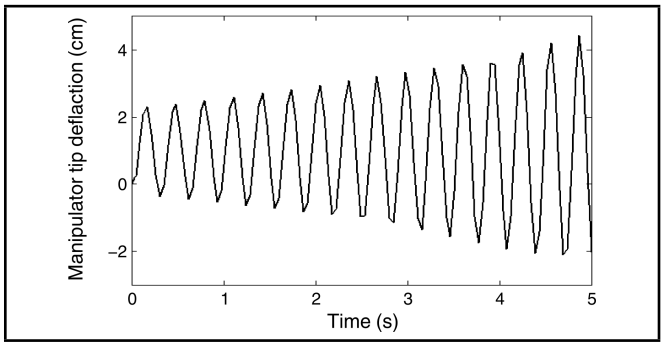

Figure 7. Manipulator tip deflection after applying the robust controller designed in the first stage.

this method, sources of uncertainty are represented by the perturbation blocks Δ_i, normalized as $\|\Delta_i\| \leq 1$. According to Fig. 4, the problem is to find the controller K that produces the control signal u to counteract the influence of w on z by minimizing the closed loop norm $\|T_{\rm wz}\|_\infty$.

Using a μ-synthesis code and a DK-iteration algorithm developed in the Robust Control Toolbox of MATLAB, an H_∞ robust controller of the 16-order is obtained. Using the same toolbox, this controller is reduced to a second order controller as follows:

$$K = \frac{1}{(s+0.005)(s+0.14)} \begin{bmatrix} s+0.24 & s+0.25 \\ s+0.51 & s+0.59 \end{bmatrix}. \quad (40)$$

Figure 15 (as seen in the Appendix) shows the Bode diagram of the 16-order and reduced second order robust controllers to validate the correctness of this approximation. The matrix transfer function $[G(s)]$ is derived from Eq. (19) as follows:

$$G(s) = \begin{bmatrix} G_{11} & G_{12} \\ G_{21} & G_{22} \end{bmatrix} = \\ = \frac{1}{D(s)} \begin{bmatrix} (\beta_2+\eta_2)s^2 + \beta_2\tilde{\omega}_2^2 & -\eta_2 s^2 \\ -\eta_1 s^2 & (\beta_1+\eta_1)s^2 + \beta_1\tilde{\omega}_1^2 \end{bmatrix}; \quad (41)$$

where $D(s)$ is given in Eq. (20). However, applying this reduced second order controller on the uncertain plant, e.g., a plant with the parameters $\beta_i = 1.2\bar{\beta}_i$, $\eta_i = 0.8\bar{\eta}_i$, and $\omega_i = \bar{\omega}_i$, $i = 1, 2$, results in an unstable time response. For instance, Fig. 7 shows the unstable time response of the manipulator tip deflection, found from Eq. (3), after applying the robust controller. The reason is that although the designed control given by Eq. (40) is stable, the transfer function $[KG^*]$ is unstable where

$$G_{11}^* = G_{21}^* = G_{11} + G_{12}; \quad (42)$$

$$G_{12}^* = G_{22}^* = G_{21} + G_{22}. \quad (43)$$

Figure 8 shows the root locus of the transfer functions $K_{11}G_{11}^*$ and $K_{22}G_{22}^*$ (root locus of the transfer functions $K_{21}G_{21}^*$ and $K_{12}G_{12}^*$ is similar to that of $K_{11}G_{11}^*$ and $K_{22}G_{22}^*$, respectively). As it is shown, due to the existence of the eigenvalues with positive real parts, using $[KG^*]$ results in unstable time responses. To overcome this problem, two more iterations are included in the μ-synthesis. After developing the

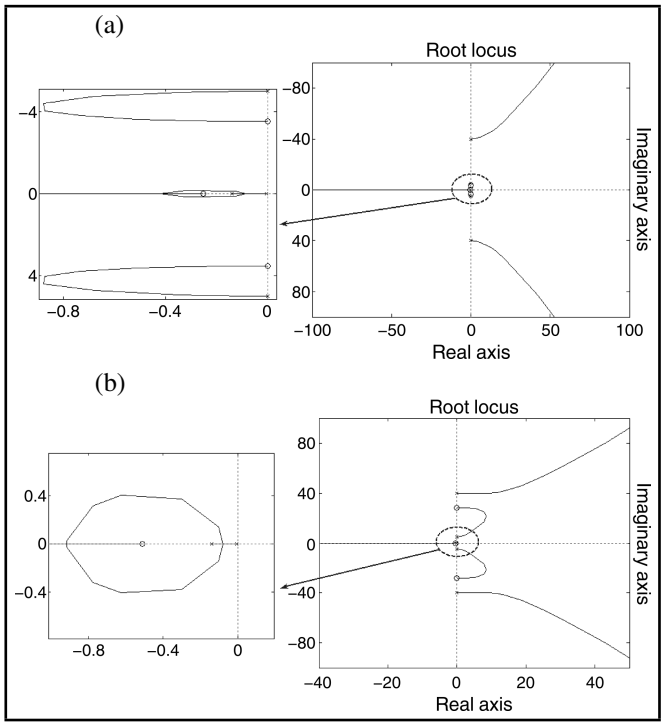

Figure 8. The root locus of the transfer functions (a) $K_{11}G_{11}^*$ (or $K_{21}G_{21}^*$) and (b) $K_{22}G_{22}^*$ (or $K_{12}G_{12}^*$).

code, the optimal robust controller is modified as follows:

$$\hat{K} = \frac{1}{(s+0.005)(s+0.14)(s+10)} \times \\ \times \begin{bmatrix} (s+0.24)(s^2+16) & (s+0.25)(s^2+1200) \\ (s+0.51)(s^2+16) & (s+0.59)(s^2+1200) \end{bmatrix}. \quad (44)$$

Figure 9 shows the root locus of the transfer functions $\hat{K}_{11}G_{11}^*$ and $\hat{K}_{22}G_{22}^*$.

Since the transfer functions $G(s)$, $\hat{K}(s)$, $\hat{K}(s)G(s)$, and consequently $S(s)$, $S(s)G(s)$, $\hat{K}(s)S(s)$, and $T(s)$ are stable, the system is nominally stable (NS).[19] Comparing Eqs. (23)–(26) and (27)–(30) shows that the condition for nominal performance (NP), robust stability (RS) and robust performance (RP) are the satisfaction of $\|W_{\rm P}S\|_\infty \leq 1$, $\|W_{\rm m}T\|_\infty \leq 1$, and $\|N\|_\infty \leq 1$, respectively. Figure 10 shows the μ-plots after applying the optimal robust controller. As it is shown, all robust stability, nominal performance, and robust performance are achieved. According to this figure, $\|W_{\rm m}T\|_\infty = 0.2$, which indicates that before the worst case uncertainty yields instability, the uncertainty may increase by a factor of $1/0.2 = 5$.

Consider that a trajectory tracking from the initial rotational angle $\theta_0 = 0$ to the final value $\theta_{\rm d} = 35°$ is desired while the manipulator tip vibration is suppressed. Figure 11 shows the rotational angle for the nominal plant and the uncertain plant with parameters, i.e., $\beta_i = 1.2\bar{\beta}_i$, $\eta_i = 0.8\bar{\eta}_i$, and $\omega_i = \bar{\omega}_i$, $i = 1, 2$. As expected, the desired characteristics of the time response, described through the performance weight in Eq. (39), are achieved. Additionally, as shown in Fig. 12, after applying the optimal robust controller, the manipulator tip vibration is suppressed. As this figure shows, during the suppression process, the uncertain plant oscillates with overall larger vibration amplitudes with respect to the nominal plant.

Figure 13 shows the μ-plot for $\|{\rm KS}\|_\infty$, which indicates no saturation in the control signal τ (because $\|KS\|_\infty \leq 1$). The

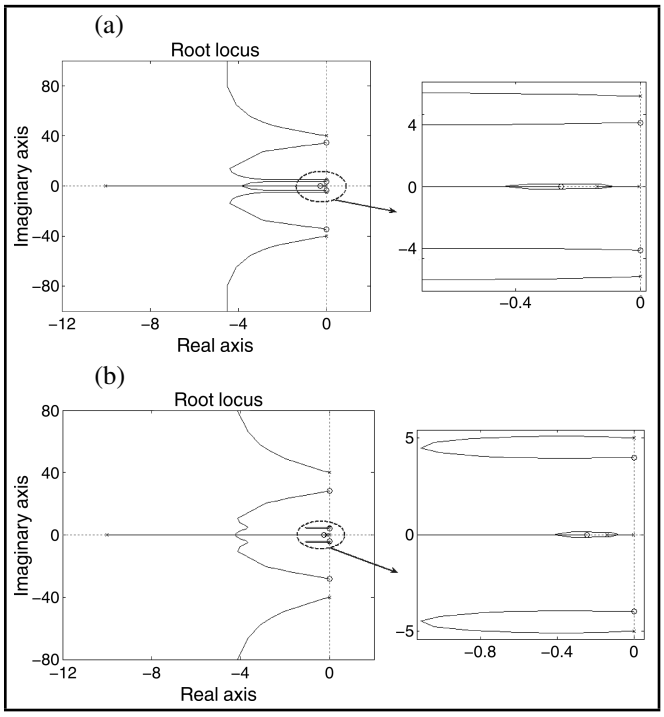

Figure 9. The root locus of the transfer functions (a) $\hat{K}_{11}G^*_{11}$ (or $\hat{K}_{21}G^*_{21}$) and (b) $\hat{K}_{22}G^*_{22}$ (or $\hat{K}_{12}G^*_{12}$).

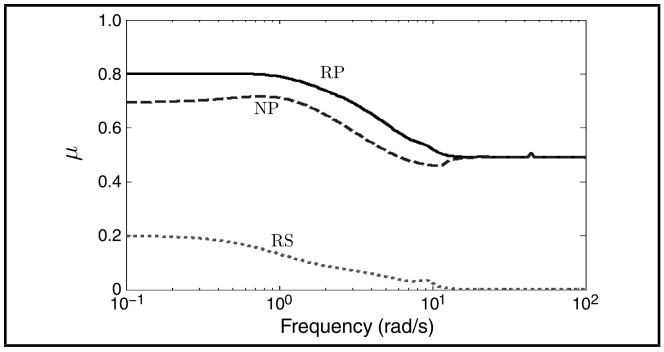

Figure 10. μ-plots of nominal performance (NP: dashed line), robust stability (RS: dots) and robust performance (RP: solid line) for the manipulator system with modified optimal robust controller.

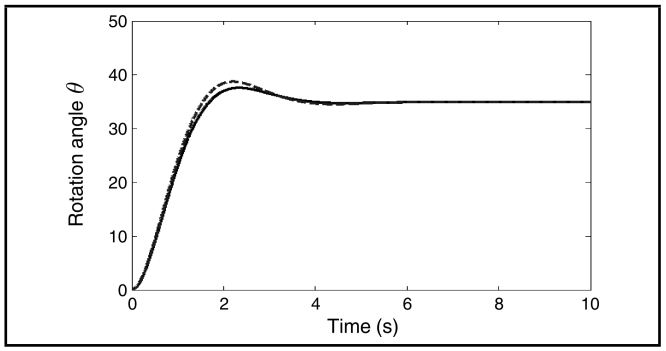

Figure 11. Rotational angle response to the desired valued $\theta_{\rm d} = 35^\circ$ for the nominal (solid line) and uncertain (dashed line) plants.

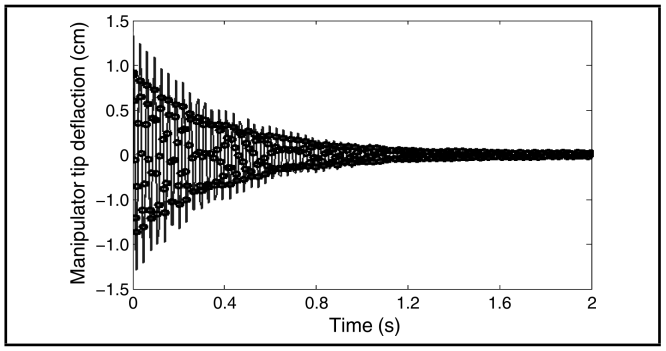

Figure 12. Manipulator tip deflection after applying the optimal robust controller for nominal (circles) and uncertain plants (solid line).

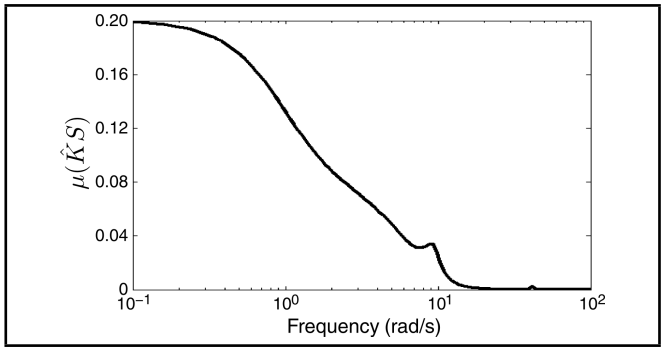

Figure 13. μ-plots for the transfer function $\hat{K}S$ with the modified optimal robust controller.

motor torque, as the control effort, is shown in Fig. 14. As it is shown and physically expected, for performance tracking and vibration suppression, the uncertain plant requires more motor torque.

It should be mentioned that the main hindrance of the proposed H_∞ control strategy is the implementation of high-order controllers, which may associate with high real-time computational load (in practice). For instance, in this research, using the proposed robust control approach leads to the 16-order controller. This controller was efficiently approximated with a second order controller, as illustrated in the Appendix (the initial controller is given by Eq. (40)). Similarly, the modified controller given by Eq. (44) is a third-order controller, obtained via reduction in a high-order one. In the majority of dynamic systems, such reduction in a controller's order is possible.[19] However, there may be some cases in which such approximation of high-order controllers to the low-order ones cannot be realized.

5. CONCLUSIONS

In this paper, an H_∞ optimal robust controller is designed to improve the performance of a rotating robotic manipulator. The Euler-Bernoulli beam theory is used to develop the dynamic model of the rotating manipulator. The mode summation technique is applied to develop the formulation in terms of general coordinates in the Laplace domain. The parametric sources of uncertainty, such as the imprecision in the payload mass and unknown properties of the manipulator link, are included.

After representation of the uncertain system in the form of the $N-\Delta$ structure, uncertainties are included in the form of multiplicative input uncertainty. The μ-synthesis control approach is used and an H_∞ robust controller is developed based on the DK-iteration algorithm. However, due to the internal instability, this controller cannot guarantee the robust stability of the uncertain system. To overcome this problem, root locus analysis is used and a modified optimal robust controller is

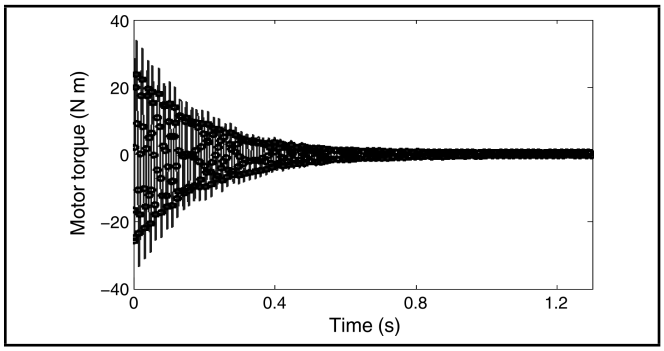

Figure 14. Required motor torque for the nominal (circles) and uncertain (solid line) plants.

designed after two more algorithm iterations.

Results show that in the presence of parametric uncertainties, robust stability and performance and nominal performance are achieved after applying the designed controller. Therefore, both the desired angular rotation and the suppression of manipulator tip vibration are achieved by manipulation of an external driving torque while the stability of the uncertain system is also guaranteed. In comparison with the nominal plant, to achieve the desired angular rotation and vibration suppression, uncertain plant requires larger motor torque.

A. LOWER AND UPPER LINEAR FRACTIONAL TRANSFORMATION

Consider a matrix P of dimension $(n_1 + n_2) \times (m_1 + m_2)$ and partition it as[19]

$$P = \begin{bmatrix} P_{11} & P_{12} \\ P_{21} & P_{22} \end{bmatrix}. \tag{45}$$

Let the matrices Δ and K have dimensions $(m_1 \times n_1)$ and $(m_2 \times n_2)$, respectively (compatible with upper and lower partitions of P). The following notation for the lower and upper linear fractional transformation is defined as:

$$F_{\mathrm{L}}(P, K) \triangleq P_{11} + P_{12}K(I - P_{22}K)^{-1}P_{21} \tag{46}$$

and

$$F_{\mathrm{u}}(P, \Delta) \triangleq P_{22} + P_{21}\Delta(I - P_{11}\Delta)^{-1}P_{12}. \tag{47}$$

B. STRUCTURAL SINGULAR VALUE

Let M be a given complex matrix and $\Delta = \mathrm{diag}\{\Delta_i\}$ denote a set of complex matrices, with $\bar{\sigma}(\Delta) \leq 1$ and a given block diagonal structure in which some of blocks may be repeated and some of the blocks may be restricted to be real. Real non-negative function $\mu(\Delta)$, called the structured singular value, is defined by[19]

$$\mu(M) = \frac{1}{\min\{k_{\mathrm{m}} | \det(I - k_{\mathrm{m}}\Delta M) = 0 \text{ for structure } \Delta; \bar{\sigma}(\Delta) \leq 1\}}.$$

If no such structured Δ exists, then $\mu(M) = 0$. A value of $\mu = 1$ means that there exists a perturbation with $\bar{\sigma}(\Delta) = 1$, which is just large enough to make $I - M\Delta$ singular. A small value of μ is desired, as it means that a larger perturbation makes $I - M\Delta$ singular.

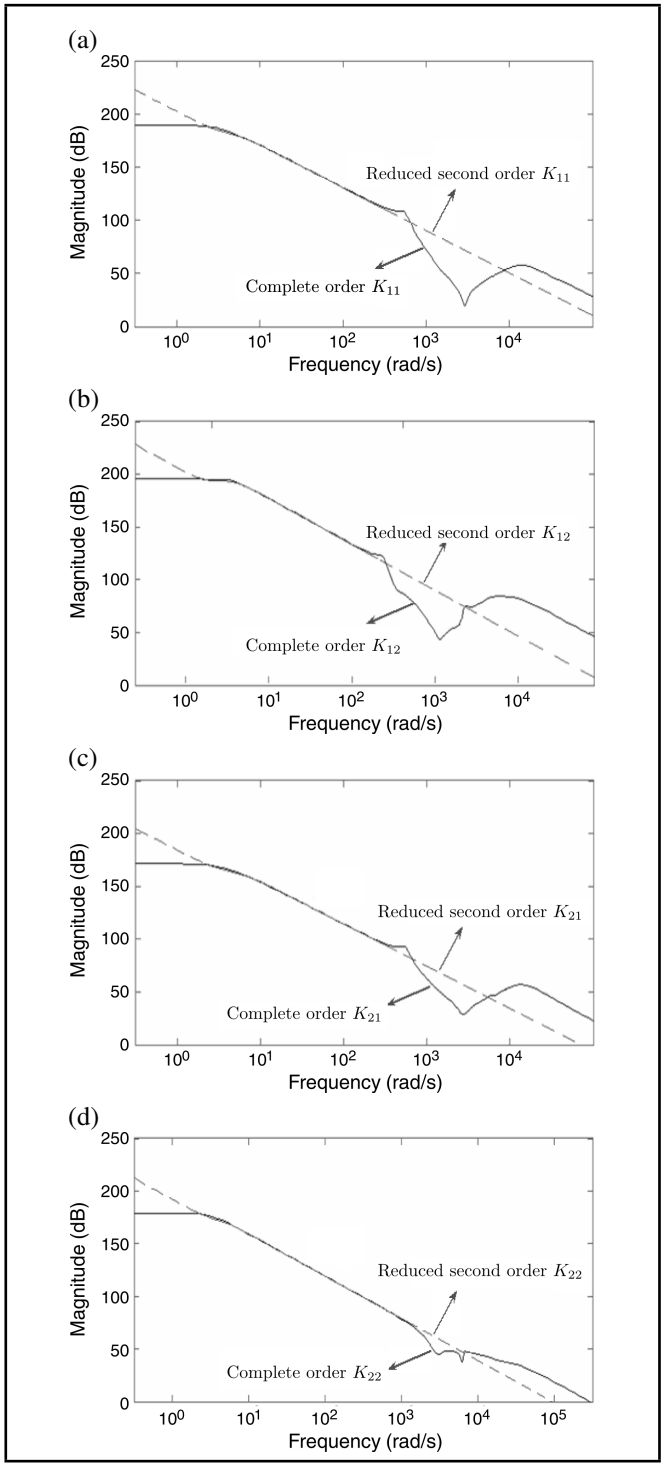

Figure 15. Bode diagrams of K_{11} (a), K_{12} (b), K_{21} (c), and $K_{22}(d)$ of the 16-order (solid line) and reduced second order (dashed line) robust controllers.

C. COMPARING THE ROBUST AND PID CONTROL APPROACHES ON THE PERFORMANCE OF THE NOMINAL PLANT

As it was already discussed, the family of classical controllers including PI, PD, and PID cannot guarantee the robust stability and performance of the model in the presence of uncertainties. Here, for the nominal plant, a comparison between the proposed robust control strategy and PID control is presented through Figs. 16–18. The Simulink Toolbox of Matlab is used for implementation of the PID controller. Due to the well-known design of PID controller, its formulation is not

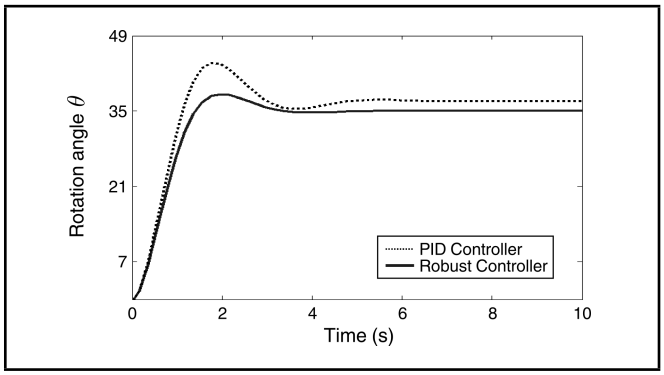

Figure 16. Rotational angle response to the desired value $\theta_{\rm d} = 35^\circ$ for the nominal model after implementation of the optimal robust controller (solid line) and a classical PID controller (dashed line).

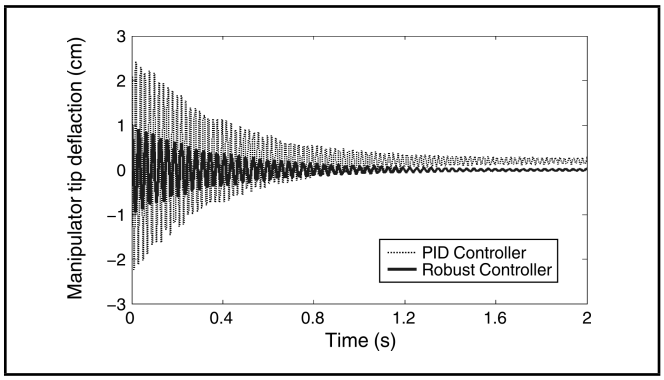

Figure 17. Manipulator tip deflection for the nominal model after implementation of the optimal robust controller (solid line) and a classical PID controller (dashed line).

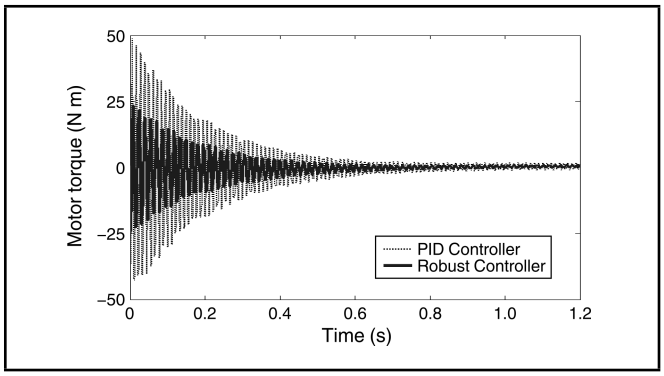

Figure 18. Required motor torque for the nominal model after implementation of the optimal robust controller (solid line) and a classical PID controller (dashed line).

presented. According to Figs. 16 and 17, when the PID controller is implemented, more oscillatory behaviour is observed for both the angular rotation and the manipulator tip deflection. In addition, time responses of these variables associate with steady state error. As it is shown in Fig. 18, more motor torque is required when the PID controller is applied.

REFERENCES

[1] DeWit, C. C., Siciliano, B., and Bastin, G. *Theory of robot control*, Springer, London, (1996).

[2] Book, W. J. Recursive Lagrangian dynamics of flexible manipulator arms, *Int. Journal of Robotic Research*, **3** (3), 87–101, (1984).

[3] Low, K. H. and Vidyasagar, M. A Lagrangian formulation of the dynamic model for flexible manipulator systems, *ASME Journal of Dynamic Systems, Measurement & Control*, **110**, 175–181, (1988).

[4] Spector, V. A. and Flasher, H. Modeling and design implications of noncolocated control in flexible systems, *ASME Journal of Dynamic Systems, Measurements & Control*, **112**, 186–193 (1990).

[5] Choura, S., Jayasuriya, S., and Medick, M. A. On the modelling, and open-loop control of a rotating thin flexible beam, *ASME Journal of Dynamic Systems, Measurement & Control,* **113**, 26–33, (1991).

[6] Yuh, J. and Young, T. Dynamic modeling of an axially moving beam in rotation: simulation and experiment, *ASME Journal of Dynamic Systems, Measurement & Control*, **113**, 34–40, (1991).

[7] Gaultier, P.E. and Cleghorn, W.L. A spatially translating and rotating beam finite element for modeling flexible manipulators, *Journal of Mechanism & Machine Theory*, **27** (4), 415–433, (1992).

[8] Matsuno, F., Asano, T., and Sakawa, Y. Modeling and quasi-static hybrid position/force control of constrained planar two-link flexible manipulators, *IEEE Transactions on Robotics & Automation*, **10**, 287–297, (1994).

[9] Benati, M. and Morro, A. Formulation of equations of motion for a chain of flexible links using Hamilton's principle, *ASME Journal of Dynamic Systems, Measurement & Control*, **116**, 81–88, (1994).

[10] Damaren, C. and Sharf, I. Simulation of flexible-link manipulators with inertial and geometric nonlinearities, *ASME Journal of Dynamic Systems, Measurement & Control*, **117**, 74–87, (1995).

[11] Fung, R.F. and Chang, H.C. Dynamic modelling of a nonlinearly constrained flexible manipulator with a tip mass by Hamilton's principle, *Journal of Sound & Vibration*, **216** (5), 751–69, (1998).

[12] Chen, W. Dynamic modelling of multi-link flexible robotic manipulators, *Journal of Computers & Structures*, **79**, 183–95, (2001).

[13] Meek, J.L. and Liu, H. Nonlinear dynamics analysis of flexible beams under large overall motions and the flexible manipulator simulation, *Journal of Computers & Structures*, **56** (1), 1–14, (1995).

[14] Kalyoncu, M. Mathematical modelling and dynamic response of a multi-straight-line path tracing flexible robot manipulator with rotating-prismatic joint, *Journal of Applied Mathematical Modelling*, **32**, 1087–1098, (2008).

[15] Bhat, S. P. and Miu, D. K. Experiments on point to point position control of a flexible beam using Laplace transform technique-part II: closed loop, *ASME Journal of Dynamic Systems, Measurement & Control*, **113**, 438–443, (1991).

[16] Diken, H. Vibration control of a rotating Euler-Bernoulli Beam, *Journal of Sound & Vibration*, **232** (3), 541–551, (2000).

[17] Gutierrez, L. B., Lewis, F. L., and Lowe, J. A. Implementation of a neural network tracking controller for a single flexible link: comparison with PD and PID controller, *IEEE Trans. Industrial Electronics*, **45** (2), 307–318, (1998).

[18] A-Ramirez, J., Cervantes, I., and Kelly, R. PID regulation of robot manipulators: stability and performance, *Journal of Systems & Control Letters*, **41**, 73–83, (2000).

[19] Skogestad, S. and Postlethwaite, I. *Multivariable Feedback Control*, John Wiley and Sons, New York, (2005).

[20] Yuan, K. and Hu, C. M. Nonlinear modeling and partial linearizing control of a slewing Timoshenko beam, *ASME Journal of Dynamic Systems, Measurement & Control*, **118**, 75–83, (1996).

[21] Green, A. and Sasiadek, J. Z. Dynamics and trajectory tracking control of a two-link robot manipulator, *Journal of Vibration & Control*, **10** (10), 1415–1440, (2004).

[22] Onsay, T. and Akay, A. Vibration reduction of a flexible arm by time optimal open-loop control, *Journal of Sound & Vibration*, **147** (2), 283–300, (1991).

[23] Su, C. Y. and Leung, T. P. A sliding mode controller with bound estimation for robot manipulators, *IEEE Trans. Robotics Automation*, **9**, 208–214, (1993).

[24] Su, C. Y. and Stepanenko, Y. Adaptive variable structure set-point control of underactuated robots, *IEEE Transaction of Automotic Control*, **44** (11), 2090–2093, (1999).

[25] Jiang, L. and Wu, Q. H. Nonlinear adaptive control via sliding model state and perturbation observer, *IEEE Proceedings of Control Theory Applications*, **149** (4), 269–277, (2002).

[26] Huang, C. Q., Peng, X. F., Jia, C. Z., and Huang, J. D. Guaranteed robustness/performance adaptive control with limited torque for robot manipulators, *Journal of Mechatronics*, **18**, 641–652, (2008).

[27] Slotine, J. E. and Li, W. Composite adaptive control of robot manipulator, *Journal of Automatica*, **25**, 509–519, (1989).

[28] Kirchoff, S. and Melek, W. W. A saturation-type robust controller for modular manipulators arms, *Journal of Mechatronics*, **17**, 175–190, (2007).

[29] Ha, Q. P., Rye, D. C., and Whyte, H. D. F. Fuzzy moving sliding mode control with application to robotic manipulators, *Journal of Automatica*, **35** (4), 607–616, (1999).

[30] Castillo, O. and Melin, P. Intelligent adaptive model-based control of robotic dynamic systems with a hybrid fuzzy-neural approach, *Journal of Applied Soft Computing*, **3**, 363–378, (2003).

[31] Melek, W. and Goldenberg, A. Neurofuzzy control of modular and reconfigurable robots, *IEEE/ASME Transactions on Mechatronics*, 381–389, (2003).

[32] Yagiz, N. and Hacioglu, Y. Robust control of a spatial robot using fuzzy sliding modes, *Journal of Mathematical & Computer Modelling*, **49**, 114–127, (2009).

[33] Sage, H.G., De Mathelin, M. F., and Ostertag, E. Robust control of robot manipulators: a survey, *Int. Journal of Control*, **72** (16), 1498–1522, (1999).

[34] Torres, S., Mendez, J. A., Acosta, L., and Becerra, V. M. On the improving the performance in robust controllers for robot manipulators with parametric disturbances, *Journal of Control Engineering Practice*, **15**, 557–566, (2007).

[35] Siqueria, A. G., Terra, M. H., and Maciel, B. C. O. Nonlinear mixed H_2/H_∞ control applied to manipulators via actuation redundancy, *Journal of Control Engineering Practice*, **14**, 327–335, (2006).

[36] Chen, B. S., Lee, T. S., and Feng, J. H. A nonlinear H_∞ control design in robotic systems under parameter perturbation and external disturbance, *Int. Journal of Control*, **59**, 439–461, (1994).

[37] Karkoub, M. and Tamma, T. Modelling and μ-synthesis control of flexible manipulators, *Journal of Computers & Structures*, **79**, 543–551, (2001).

[38] Mohamed, Z. and Tokhi, M. O. Command shaping techniques for vibration control of a flexible robot manipulator, *Journal of Mechatronics*, **14**, 69–90, (2004).

[39] White, M. W. and Heppler, G. R. Vibration of a rotating Timoshenko beam, *ASME Journal of Vibration & Acoustics*, **118**, 607–613, (1996).

[40] Inman, D. J. *Engineering Vibration*, Prentice Hall Int. Inc., Englewood, NJ, (1994).